Resilience Analysis and Cascading Failure Modeling of Power Systems Under Extreme Temperatures

Seyyed Rashid Khazeiynasab, *Student Member*, *IEEE* and Junjian Qi, *Senior Member*, *IEEE*

***Abstract*—In this paper, we propose an AC power flow based cascading failure model that explicitly considers external weather conditions, extreme temperatures in particular, and evaluates the impact of extreme temperature on the initiation and propagation of cascading blackouts. Based on this model, resilience analysis of the power system is performed with extreme temperatures. Specifically, the changes of load and dynamic line rating are modeled due to temperature disturbance. The probabilities for transmission line and generator outages are evaluated, and the timing for each type of events is calculated to decide the actual event sequence. It should be emphasized that the correlated events, in the advent of external temperature changes, could contribute to voltage instability. Besides, we model undervoltage load shedding and operator re-dispatch as control strategies for preventing the propagation of cascading failures. The effectiveness of the proposed model is verified by simulation results on the RTS-96 3-area system. It is found that temperature disturbances can lead to correlated load change and line/generator tripping, which will greatly increase the risk of cascading and voltage instability. Critical temperature change, critical area with temperature disturbance, the identification of most vulnerable buses, and the comparison of different control strategies are also investigated.**

***Index Terms*—Blackout, cascading failure, correlation, extreme temperature, extreme weather, power transmission reliability, resilience, voltage stability.**

I. Introduction

CASCADING failure is a common phenomenon in both natural and engineered systems such as electric power systems [1], natural gas systems [2], transportation networks [3], disease transmission networks [4], and interdependent networks [5]-[7]. For example, there have been several large-scale blackouts such as the 2003 U. S. -Canadian blackout [8], the 2011 Arizona-Southern California blackout [9], and the 2012 Indian blackout [10], which have led to extensive outage propagations and significant impacts [11]. In order to simulate and analyze the cascading failures, many models with different levels of details have been developed [1] such as Manchester model [12], hidden failure model [13], [14], CASCADE model [15], optimal power allocation (OPA) model [16], AC OPA model [17], dynamic model [18], cascading failure model with detailed protection systems [19], sandpile model [20], branching process model [21], [22], multi-type branching process model [23], interaction model [24]-[28], and Markovian influence graph [29].

However, the existing models mainly focus on the system itself, usually ignoring the interactions between the system and various external factors such as extreme weather conditions. These factors are important for both initiation and propagation of cascading failures. For U.S.-Canadian blackout on August 14, 2003, the temperature was as high as 31 ℃, causing load increase in FirstEnergy's control area, transmission line tripping due to tree contact, and generator tripping due to increased reactive power outputs [8]. Another blackout occurred partly because of temperature disturbance on July 2, 1996. High loads in Southern Idaho and Utah, USA, due to high temperature around 38 ℃ [30], [31] led to high demands and subsequently highly loaded transmission lines.

In recent years, a few papers have investigated the impact of temperature on cascading failure risks. In [32], a stochastic model is proposed in which random line failures are generated at constant failure rates and overloaded line failures occur when the line temperature reaches the equilibrium temperature. In [33], an OPA model with slow process is proposed in which the line temperature evolution is modeled for calculating the line length and sag changes in order to evaluate the possibility for tree contact or damage. In [34], a probabilistic risk assessment (PRA) model is developed to consider the impact of wind speed and the evolution of line temperature. In [35], risk assessment of weather-related cascading outages is presented based on weather-dependent outage rates. In [36], historical outage data is used to estimate the effects of the weather on cascading failure, and bulk statistics of historical initial line outages are provided. However, all these existing models have the following problems.

1) The initiation events are still generated by random sampling, which does not consider the important geographical correlations of the initiation events due to external weather conditions such as temperature disturbance.

Manuscript received: January 11, 2020; accepted: June 11, 2020. Date of CrossCheck: June 11, 2020. Date of online publication: October 1, 2020.

This work was supported by National Science Foundation (No. CAREER 1942206).

S. R. Khazeiynasab and J. Qi (corresponding author) are with the Department of Electrical and Computer Engineering, University of Central Florida, Orlando, FL 32816, USA (e-mail: rashid@knights.ucf.edu; jqi8@stevens.edu).

DOI: 10.35833/MPCE.2020.000016

2) Ambient temperature disturbance at various geographical locations in the system is not explicitly modeled, and the changes of consequent demand and dynamic line rating are not modeled, which are critical for understanding the initiation and propagation of cascading failures, especially due to the loss of voltage stability.

Therefore, to better understand the cascading failure, it is needed to develop a model that explicitly considers the ambient temperature disturbances and their impacts on cascading failure risks. The contributions of this paper are listed below.

1) We develop a cascading failure model that explicitly considers ambient temperature disturbances and the subsequent demand changes and dynamic line rating changes, considering the correlation between different events such as line outage, generator tripping, and undervoltage of load buses. Besides, the control strategies are modeled against failure propagation such as undervoltage load shedding and operator re-dispatch.

2) Based on the proposed cascading failure model, we provide an explanation about why the failure can still be initiated and propagated even when the power system is initially $N-1$ secure by considering the impact of ambient temperature disturbances and the correlation between different events.

3) We perform risk assessment for power systems based on the proposed model to investigate critical temperature change and critical area with temperature disturbance, which could lead to significantly increased risk of cascading failures, identify the most vulnerable buses for temperature disturbances, and evaluate the effectiveness of different control strategies on reducing the system risk.

The remainder of this paper is organized as follows. Section II discusses ambient temperature disturbance, models load and line rating changes due to temperature change, and evaluates the probabilities of transmission line and generator tripping. Control strategies including undervoltage load shedding and operator re-dispatch are modeled in Section III. Section IV determines the timing of different types of events, and Section V introduces the calculation of voltage stability margin. In Section VI, the proposed blackout model is summarized. Section VII tests and validates the proposed model on the RTS-96 3-area system. Finally, conclusions are drawn in Section VIII.

II. Ambient Temperature in Blackout Modeling

Assume there are n buses in a power system, including a slack bus that is numbered as i_s. The vector of ambient temperatures of all buses is $\boldsymbol{T}=[T_1, T_2, \ldots, T_n]^{\mathrm{T}}$. The vector of ambient temperatures of the load buses is denoted by $\boldsymbol{T}_{S_L}$. For a transmission line l: $i \to j$ that connects bus i and bus j and crosses M areas, its ambient temperature is assumed to be dependent on the temperatures of the M areas.

A. Temperature Disturbance

An ambient temperature disturbance is applied to an area $\boldsymbol{A}=\left[\underline{\phi}, \overline{\phi}\right] \times \left[\underline{\lambda}, \overline{\lambda}\right]$, where $\overline{\phi}$ and $\underline{\phi}$ are the upper and lower bounds for the latitude in area A, respectively; and $\overline{\lambda}$ and $\underline{\lambda}$ are the upper and lower bounds for the longitude in area A, respectively. In order to make sure that at least one load bus is inside the chosen area, we randomly select a load bus and an area around this bus. The chosen area is set to be $\underline{\phi}=\phi_c-\Delta\phi$, $\overline{\phi}=\phi_c+\Delta\phi$, $\underline{\lambda}=\lambda_c-\Delta\lambda$, and $\overline{\lambda}=\lambda_c+\Delta\lambda$, where ϕ_c and λ_c are the longitude and latitude of the selected load bus, respectively; and $\Delta\phi>0$ and $\Delta\lambda>0$ determine how widespread the disturbance is and are defined as:

$$\Delta\phi=\gamma(\phi^{\max}-\phi^{\min}) \tag{1}$$

$$\Delta\lambda=\gamma(\lambda^{\max}-\lambda^{\min}) \tag{2}$$

where γ is a constant ($0<\gamma\le 1$) and defines the size of area k; $\phi^{\max}$ and $\phi^{\min}$ are the maximum and minimum latitudes among all buses, respectively; and $\lambda^{\max}$ and $\lambda^{\min}$ are the maximum and minimum longitudes among all buses, respectively. As a disturbance, the ambient temperature of the load buses in the selected subsystem is changed by ΔT. Obviously, the ambient temperature of the transmission lines in the selected subsystem will also change by ΔT. For a line l:$i \to j$ that crosses the boundary of the selected area and lies in M areas, its length in area k with ambient temperature of T_k is d_k, and its temperature is determined by:

$$T_{ij}=\frac{1}{D_{ij}}\sum_{k=1}^{M}T_k d_k \tag{3}$$

where D_{ij} is the distance between buses i and j, and bus i is assumed to be inside the selected area while bus j is not. As a simple case, for a line l:$i \to j$ that only crosses two areas, its temperature is given as:

$$T_{ij}=\frac{d_1}{D_{ij}}T_i+\frac{d_2}{D_{ij}}T_j \tag{4}$$

where d_1 and d_2 are the lengths of the line in and out of the selected area, respectively. Then with a ΔT change for bus i, the ambient temperature of the line l:$i \to j$ will change by:

$$\Delta T_{ij}=\frac{d_1}{D_{ij}}\Delta T \tag{5}$$

To calculate the distance between two buses, we assume that the earth is a sphere with a radius of 6378 km. Let the central angle Θ between two buses i and j be:

$$\Theta=\frac{D_{ij}}{R} \tag{6}$$

where R is the radius of the earth.

The haversine function of Θ [37] and the haversine function of an angle θ are:

$$hav(\Theta)=hav(\Delta\phi_{i,j}^{d})+\cos\phi_i\cos\phi_j\, hav(\Delta\lambda_{i,j}^{d}) \tag{7}$$

$$hav(\theta)=\sin^2\left(\frac{\theta}{2}\right) \tag{8}$$

where $\Delta\phi_{i,j}^{d}$ and $\Delta\lambda_{i,j}^{d}$ are the differences between the latitude and the longitude of buses i and j, respectively.

Finally, by applying the inverse haversine hav^{-1} to the central angle Θ, we can find the distance $D_{ij}=2R\arcsin\left(\sqrt{\sin^2\left(\Delta\phi_{i,j}^{d}/2\right)+\cos\phi_i\cos\phi_j\sin^2\left(\Delta\lambda_{i,j}^{d}/2\right)}\right)$.

Note that a relatively large ambient temperature change could take a few hours during which some protections may

operate. However, from the perspective of modeling, it may be too complicated if we consider the temporal behavior of the ambient temperature change and its impact on the risk of cascading failures. Therefore, we consider a simplified scenario in which the ambient temperature change happens immediately. And we focus more on what impact it will have on system operation and cascading failure risks.

B. Load Change with Temperature Disturbances

In power systems, load forecasting is used for day-ahead generation purchase and reactive power management. However, due to uncertainties, the actual load may be different from the forecasted load. For example, several large operators in the Midwest, USA consistently under-forecasted the load levels between August 11 and 14, 2003 [8]. We assume the initial ambient temperature for all load bus T_0 is used for day-ahead load forecasting while the actual ambient temperature for a subsystem is $T_0+\Delta T$, which will lead to a deviation of actual load from the forecasted load.

The real power of a load bus i changes with its ambient temperature T_i as:

$$P_i = L_{P_i}(T_i)P_{0,i} \tag{9}$$

where T_i is the ambient temperature where bus i is located; and $P_{0,i}$ is the nominal real power at bus i. Without the loss of generality, we assume $L_{P_i}(T_i)=L(T_i)$, where the same function L is used for all buses. According to [38]-[40], $L(T_i)$ can be represented by a polynomial function as $L(T_i)=a_3T_i^3+a_2T_i^2+a_1T_i+a_0$.

In Fig. 1, the fitted function L is shown as the red line for the Greek interconnected power system based on the data between January 1, 1993 and December 31, 2003 [39], [40]. It shows that the load variation with the temperature is nonlinear and asymmetrically increases for decreased or increased temperatures with a minimum at around $T_{\min}=18.5$ ℃ [39], [40]. The load is more sensitive to higher temperature increase than to lower temperature decrease, since several energy sources such as diesel, natural gas, electricity can be used for heating, while only the electricity can be used for cooling practically [39], [40]. A similar curve can be found in [38]. Assume the initial load to be the ambient temperature that leads to $L(T)=1$. For example, if we use the curve in Fig. 1, there will be two corresponding positive ambient temperatures, which are the low temperature $T_{0,low}=9.91$ ℃ and the high temperature $T_{0,high}=24.21$ ℃, respectively. If we want to explore the effect of temperature increase or decrease, we will assume that the ambient temperature corresponding to the initial load is $T_0=T_{0,high}$ ($T_0=T_{0,low}$).

With high or low temperatures, there will be more air conditioning loads which consume more reactive power and have lower power factors than other types of loads [8]. Accordingly, we assume that the power factor linearly decreases with the temperature increase as $pf_i=pf_{0,i}-k_i^{pf}(T_i-T_0)$ when $T_0=T_{0,high}$ and $T_i\geq T_{\min}$ and $pf_i=pf_{0,i}+k_i^{pf}(T_i-T_0)$ when $T_0=T_{0,low}$ and $T_i\leq T_{\min}$, where pf_i is the power factor of bus i and $pf_{0,i}$ is the initial power factor under initial temperature of bus i.

Then, the reactive power of load bus i with temperature T_i can be obtained as:

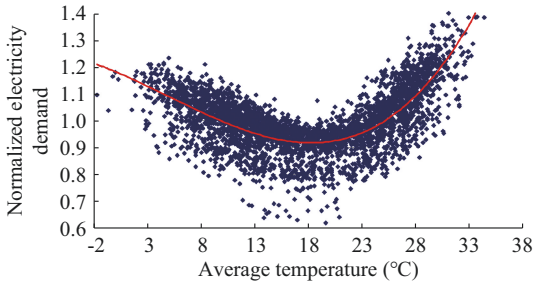

Fig. 1. Relationship between normalized electricity demand and temperature for the Greek power system based on data between January 1, 1993 and December 31, 2003.

$$Q_i = P_i \tan(\arccos(pf_i)) \tag{10}$$

where P_i is the real power of load bus i.

C. Dynamic Line Rating

Assume the initial rating of a transmission line $l{:}i\rightarrow j$ is determined for the initial temperature $T_{0,ij}=(T_{0,i}+T_{0,j})/2$. When the scenario for the high temperature is investigated, $T_{0,ij}=T_{0,high}=24.21$ ℃. This is consistent with the fact that the approximate current carrying capacity is usually 25 ℃ [41].

The dynamic line rating can depend on the ambient temperature [42] and utility management vegetation [33]. According to [42], the effect of ambient temperature on the dynamic line rating expressed in Ampere is quasi-linear. Therefore, for the dynamic line rating expressed in apparent power (MVA), we can obtain:

$$\overline{F}_{ij}^{d} = V_{ij}^{rated}V_{ij}(-k_{ij}T_{ij}+c_{ij}) \tag{11}$$

where V_{ij}^{rated} and V_{ij} are the nominal voltage and per-unit voltage of line $l{:}i\rightarrow j$, respectively; and k_{ij} is the slope. Different conductors may have different k_{ij}. For example, the slope for the AMS570 conductor is approximately 0.02 kA/℃ [42]. For simplicity, we use the same slope $k_{ij}=0.02$ kA/℃ for all lines. Then c_{ij} can be easily obtained as $c_{ij}=\overline{F}_{0,ij}/(V_{ij}^{rated}V_{0,ij})+k_{ij}T_{0,ij}$.

In order to consider the utility vegetation management and the corresponding risk for line tripping due to a slow process involving transmission line temperature evolution, sag increase, and tree contact [33], (11) can be modified as:

$$\overline{F}_{ij}^{d} = \alpha_{ij}V_{ij}^{rated}V_{ij}(-k_{ij}T_{ij}+c_{ij}) \tag{12}$$

where α_{ij} is uniformly sampled in $[\underline{\alpha},1]$ with $0<\underline{\alpha}\leq 1$. When $\alpha_{ij}=1$, the dynamic line rating is only determined by the ambient temperature.

D. Line Tripping Probability

For a line $l{:}i\rightarrow j$, let $R_{ij}(T)=F_{ij}(T_{S_L})/\overline{F}_{ij}^{d}(T_{ij})$. Note that F_{ij} is a function of the ambient temperatures of the load buses and will change when there is a load change at any load bus due to the ambient temperature change. By contrast, the dynamic line rating $\overline{F}_{ij}^{d}$ is only a function of the local ambient temperature of the line $l{:}i\rightarrow j$.

The line tripping probability P_{ij}^{trip} can be written as a function of R_{ij}:

$$P_{ij}^{trip} = f_t(R_{ij}(T)) \tag{13}$$

In this paper, we propose the function shown in Fig. 2 for the line tripping probability, which can be written as:

$$f_t = \begin{cases} p_1 & R_{ij} \le 1 \\ a_1 e^{b_1 R_{ij}} & 1 < R_{ij} \le 1+\epsilon \\ a_2 e^{b_2 R_{ij}} & 1+\epsilon < R_{ij} \le K \\ p_3 & R_{ij} > K \end{cases} \tag{14}$$

where $b_1 = (\ln p_1 - \ln p_2)/(-\epsilon)$, $a_1 = p_1/e^{b_1}$, $b_2 = (\ln p_2 - \ln p_3)/(1+\epsilon - K)$, and $a_2 = p_2/e^{b_2(1+\epsilon)}$. When $R_{ij} \le 1$, although there is no slow process involved, a line may still be tripped by a small probability, by which we can consider the factors could lead to line tripping even if the dynamic line rating is not reached. For example, even if F_{ij} is far below $\overline{F}_{ij}^{d}$, the line may be tripped by the protection due to lighting strikes, then the line tripping probability is not equal to zero, but is equal to a constant low value to describe the tripping probability of a line exposed to a hidden failure. Once $R_{ij} > 1$, it becomes possible for the line to be tripped such as due to tree contact or overheating and the tripping probability. Then the line quickly grows to a much higher value p_2 at $R_{ij} = 1+\epsilon$. Then when R_{ij} is between $1+\epsilon$ and K, the line tripping probability increases exponentially with the parameters a_2 and b_2. Finally, it reaches to a high probability $p_3 \le 1$ when R_{ij} is greater than K. In this paper, we set p_3 to be 1.

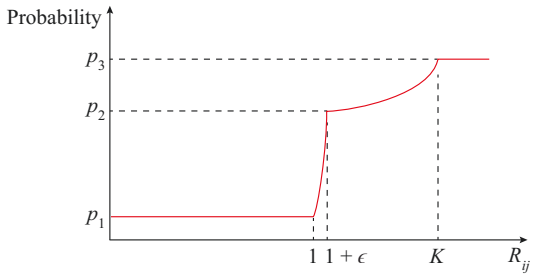

Fig. 2. Line tripping probability as a function of R_{ij}.

E. Generator Tripping Probability

The active power change due to the ambient temperature change is $\Delta P = \sum_{i \in S_L^A} (P_i - P_{0,i})$, where S_L^A is the set of load buses within the selected area. This change will be supplied by all generators in proportion to their active power reserve. Specifically, for $i \in \mathcal{S}_G \backslash i_s$, where $\mathcal{S}_G$ is the set of generator buses, we can obtain:

$$P_i = P_{0,i} + \frac{\overline{P}_i - P_{0,i}}{\sum_{i \in \mathcal{S}_G} (\overline{P}_i - P_{0,i})} \Delta P \tag{15}$$

When reactive load increases, the generators nearby will have to provide more reactive power. For example, in 2003 U. S. -Canadian blackout, Eastlake unit 5 in FirstEnergy's Northern Ohio service area was generating high reactive power, because there were significant reactive power supply problems in the states of Indiana and Ohio, USA. Due to high reactive output and overexcitation, this unit was tripped [8].

Automatic voltage regulator is assumed to be equipped for each generator to hold the terminal voltages. Normally, there is no automatic control action limiting the reactive power output of generators [43], and the reactive power of a generator can be beyond the allowed capacity range $[\underline{Q}_i, \overline{Q}_i]$ due to voltage regulation to relieve the overvoltage or undervoltage violations close to the generator. Note that $\underline{Q}_i$ and $\overline{Q}_i$ are the lower and upper reactive power capacities for generator i, respectively. In this paper, we consider the increased possibility of generator tripping due to overexcitation limiter operation. The tripping probability of the generator i can be written as a function of Q_i as:

$$P_i^{trip} = f_g(Q_i) \tag{16}$$

$$f_g(Q_i) = \begin{cases} p_6 & Q_i \le \underline{K}_{Q_i} \\ a_3 e^{b_3 Q_i} & \underline{K}_{Q_i} < Q_i \le \underline{Q}_i - \underline{\epsilon} \\ a_4 e^{b_4 Q_i} & \underline{Q}_i - \underline{\epsilon} < Q_i \le \underline{Q}_i \\ p_4 & \underline{Q}_i < Q_i \le \overline{Q}_i \\ a_5 e^{b_5 Q_i} & \overline{Q}_i < Q_i \le \overline{Q}_i + \overline{\epsilon} \\ a_6 e^{b_6 Q_i} & \overline{Q}_i + \overline{\epsilon} < Q_i \le \overline{K}_{Q_i} \\ p_6 & Q_i > \overline{K}_{Q_i} \end{cases} \tag{17}$$

where $b_3 = (\ln p_6 - \ln p_5)/(\underline{K}_{Q_i} - \underline{Q}_i + \underline{\epsilon})$, $a_3 = p_6/e^{b_3 \underline{K}_{Q_i}}$, $b_4 = (\ln p_5 - \ln p_4)/(-\underline{\epsilon})$, $a_4 = p_5/e^{b_4(\underline{Q}_i - \underline{\epsilon})}$, $b_5 = (\ln p_4 - \ln p_5)/(-\overline{\epsilon})$, $a_5 = p_4/e^{b_5 \overline{Q}_i}$, $b_6 = (\ln p_5 - \ln p_6)/(\overline{Q}_i + \overline{\epsilon} - \overline{K}_{Q_i})$, and $a_6 = p_5/e^{b_6(\overline{Q}_i + \overline{\epsilon})}$. If the reactive power of any generator i lies in $[\underline{Q}_i, \overline{Q}_i]$, it fails only by a very small probability p_4 in order to model any accidental failure. When Q_i falls out of $[\underline{Q}_i, \overline{Q}_i]$, the generator tripping probability quickly grows to a much higher value p_5 at $\underline{Q}_i - \underline{\epsilon}$ or $\overline{Q}_i + \overline{\epsilon}$. Then, from $\underline{K}_{Q_i}$ to $\underline{Q}_i - \underline{\epsilon}$ or from $\overline{Q}_i + \overline{\epsilon}$ to $\overline{K}_{Q_i}$, the tripping probability increases exponentially with parameters a_3, b_3 and a_6, b_6, respectively. Finally, when $Q_i \le \underline{K}_{Q_i}$ or $Q_i > \overline{K}_{Q_i}$, it reaches a high probability p_6 for the most abnormal cases.

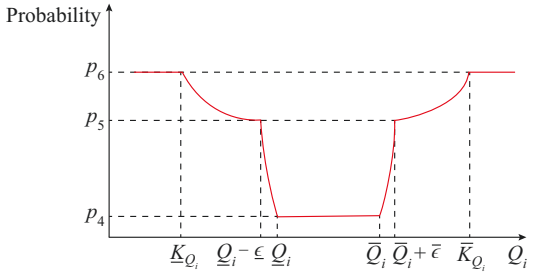

Fig. 3. Generator tripping probability as a function of Q_i.

III. Modeling Protection and Control Strategies

A. Undervoltage Load Shedding

When the voltage of a load bus i is below a threshold V_{th}

for more than τ s, a portion of the real power load will be shed [44]. The amount of active power to be shed is determined as:

$$\Delta P_{sh,i} = \min(K_{sh}\Delta V_i, P_i) \tag{18}$$

where K_{sh} is the load shedding constant; and $\Delta V_i = V_{th} - V_i > 0$. In this paper, the parameters are chosen as $V_{th} = 0.9$ p.u., $K_{sh} = 600$ MW per unit, and $\tau = 3$ s. In order to preserve the power factor, the reactive power to be shed is calculated as [45]:

$$\Delta Q_{sh,i} = Q_i \frac{\Delta P_{sh,i}}{P_i} \tag{19}$$

B. Operator Re-dispatch

Note that the operator only has the initial branch flow capacity $\overline{F}_{ij}^0$. If the branch flow is greater than the dynamic rating but smaller than $\overline{F}_{ij}^0$, the operator will not perform any re-dispatch. Only when the line flow is higher than $\overline{F}_{ij}^0$ will the operator be able to perform a shift-factor S based re-dispatch, which well reflects the actual operator's behavior.

Assume line l: $i \to j$ is overloaded, i.e., $F_{ij} > \overline{F}_{ij}^0$. We select n^+ generators $\{G_{P_1}, G_{P_2}, \ldots, G_{P_{n^+}}\}$ with positive shift factors and n^- generators $\{G_{N_1}, G_{N_2}, \ldots, G_{N_{n^-}}\}$ with negative shift factors. For the generators with positive shift factors, without the loss of generality, we assume:

$$S_{P_1} \geq S_{P_2} \geq \ldots \geq S_{P_{n^+}} \tag{20}$$

To reduce the line overloading the most effectively, the generators with positive shift factors should be dispatched, i.e., decreasing their outputs, in the order of $G_{P_1}, G_{P_2}, \ldots, G_{P_{n^+}}$. Specifically, for generator G_{P_i}, $i = 1, 2, \ldots, n^+$, its real power output is re-dispatched as:

$$P_{P_i} = P_{0,P_i} + \frac{\eta(\overline{F}_{ij}^0 - F_{ij})}{S_{P_i}} \tag{21}$$

If the generators with positive shift factors cannot eliminate the overloading, the generators with negative shift factors will be re-dispatched. Without the loss of generality, we assume:

$$S_{N_1} \leq S_{N_2} \leq \ldots \leq S_{N_{n^-}} \tag{22}$$

These generators are dispatched, i.e., increasing their outputs, in the order of $G_{N_1}, G_{N_2}, \ldots, G_{N_{n^-}}$ by a similar approach to that for the generators with positive shift factors.

If there are multiple overloaded branches, the above re-dispatch will be applied to each of them according to F_{ij}/F_{ij}^0. The larger F_{ij}/F_{ij}^0 of a branch is, the earlier the overloading of this branch will be dealt with by the re-dispatch of generators. If necessary, multiple rounds of the re-dispatch will be executed until the overloading of all branches is eliminated or the number of rounds reaches a limit.

IV. Timing of Events

Define a set of events for iteration $k+1$ as $E = \{e_1, e_2, \ldots, e_m\}$, where m is the number of potential events that could happen in iteration $k+1$. The events could be with low voltage of a load bus, tripping of a line whose F_{ij} could be smaller or greater than its dynamic rating $\overline{F}_{ij}^d$, and tripping of a generator whose reactive power output is within or exceed its lower and upper limits. Each type of events will fail after a specific amount of time which will be decided as follows.

As mentioned in Section III-A, when the voltage of a load bus i is below a pre-defined threshold for more than $\tau = 3$ s, we shed ΔP_i^{sh} and ΔQ_i^{sh} of the load at bus i. The re-dispatch in Section III-B is assumed to be be finished in 1 min. If a line whose F_{ij} is smaller than its dynamic line rating $\overline{F}_{ij}^d$ is tripped, there is no slow process involved and the line is disconnected by the protective relay after a very short time, which may include the operation time of the relay and breaker. We set this time to be 0.2 s [46].

When $F_{ij} \geq \overline{F}_{ij}^d$, the line may be tripped for different reasons such as tree contact caused by a slow process [8], [33], overheating, or mis-operation of zone 2 and zone 3 of distance relays [8]. The time of line tripping under different mechanisms can vary significantly. For example, in the 2003 U.S.-Canadian blackout the Stuart-Atlanta 345 kV line tripping took 31 min due to tree contact. The backup zone 2 and zone 3 relay can operate in a few seconds. The probability of a line with $F_{ij} \geq \overline{F}_{ij}^d$ to fail can be determined based on Section II-D. If such a line l:$i \to j$ is to fail, it fails when its total accumulated overload exceeds a limit $\bar{o}_{ij}$ which represents the condition required for line tripping due to a number of processes such as the overheating of a transmission line or the sagging of the line to vegetation [33], [47]. Let $\Delta o_{ij,0} = 0$. The time for line l:$i \to j$ whose F_{ij} is greater than $\overline{F}_{ij}^d$ in iteration $k+1$ can be calculated as:

$$\Delta t_{ij,k+1} = \frac{\bar{o}_{ij} - \sum_{m=0}^{k} \Delta o_{ij,m}}{F_{ij}(t_k) - \overline{F}_{ij}^d(t_k)} \tag{23}$$

where the limit $\bar{o}_{ij}$ is chosen so that a branch will trip after 20 s, which is 50% above the branch flow limit; and $\Delta o_{ij,m}$ is the accumulated overload in iteration m between t_{m-1} and t_m for line l:$i \to j$.

According to [43], generators usually have about 10%-20% overload capability for up to 30 min. We use a similar approach to determine the time for generator tripping in every interval. When the reactive power of a generator g is in $[\underline{Q}_g, \overline{Q}_g]$, it fails by a very small probability p_1 because of accidental failure. $\overline{Q}_g$ and $\underline{Q}_g$ are the upper and lower reactive power capacities for generator g, respectively. For these types of failures, we set the time to be 0.2 s [48]. If the reactive power of generator g moves out of $[\underline{Q}_g, \overline{Q}_g]$, the probability for that generator to fail can also be determined by Section II-E. If the generator is to fail, the time that is required for this generator to fail at iteration $k+1$ can be calculated as:

$$\Delta t_{g,k+1}=\begin{cases}\dfrac{\bar{o}_g-\sum_{m=0}^{k}\Delta o_{g,m}}{\underline{Q}_g-Q_g(t_k)} & Q_g<\underline{Q}_g\\ \dfrac{\bar{o}_g-\sum_{m=0}^{k}\Delta o_{g,m}}{Q_g(t_k)-\overline{Q}_g} & Q_g>\overline{Q}_g\end{cases} \tag{24}$$

where $\Delta o_{g,m}$ is the accumulated overload in iteration m between t_{m-1} and t_m, for generator g; and $\bar{o}_g$ is the chosen threshold so that a generator will trip after 30 min of being 20% above/below the upper/lower reactive power limit and $o_{g,0}=0$.

Let $\Delta t_{k+1}^{\min}$ be the minimum time of all events in iteration $k+1$, and it can be calculated as:

$$\Delta t_{k+1}^{\min}=\min t(e_i)\quad i=1,2,\ldots,m \tag{25}$$

where $t(e_i)$ is the time for event e_i; and the time corresponding to the next event is $t_{k+1}=t_k+\Delta t_{k+1}^{\min}$.

Δo_{ij} at iteration $k+1$ can be obtained by [47]:

$$\Delta o_{ij,k+1}=\max(F_{ij}(t_k)-\overline{F}_{ij}^{d}(t_k),0)\Delta t_{k+1}^{\min} \tag{26}$$

Δo_g at iteration $k+1$ can be calculated as $\Delta o_{g,k+1}(\underline{Q}_g-Q_g(t_k))\Delta t_{k+1}^{\min}$ when $Q_g<\underline{Q}_g$ and $\Delta o_{g,k+1}(Q_g(t_k)-\overline{Q}_g)\Delta t_{k+1}^{\min}$ when $Q_g>\overline{Q}_g$.

V. Calculation of Voltage Stability Margin

Voltage instability has been responsible for several major blackouts such as New York Power Pool disturbance on September 22, 1970 and Western Systems Coordination Council (WSCC) transmission system disturbance on July 2, 1996.

A system enters a state of voltage instability when a disturbance such as a load increase or change in system conditions causes a progressive and uncontrollable voltage decline. In blackouts, the load increases due to temperature disturbance and the reactive power supply decreases due to the increased tripping probabilities of the lines and generators that are geographically close to the load increase area. More importantly, the load increase and the increase of line tripping probability are correlated and both are related to the temperature disturbance, which may greatly increase the risk of failures.

After each change in the operation condition, we calculate the voltage stability margin based on the QV index proposed in [49]. Specifically, for a power flow model:

$$\begin{bmatrix}\Delta P\\ \Delta Q\end{bmatrix}=\begin{bmatrix}J_{P\theta} & J_{PV}\\ J_{Q\theta} & J_{QV}\end{bmatrix}\begin{bmatrix}\Delta\theta\\ \Delta V\end{bmatrix} \tag{27}$$

Let $\Delta P=0$, we can obtain:

$$\Delta\theta=-J_{P\theta}^{-1}J_{PV}\Delta V \tag{28}$$

Substituting (28) into the ΔQ in (27), we can obtain:

$$\Delta Q=(J_{QV}-J_{QB}J_{P\theta}^{-1}J_{PV})\Delta V \tag{29}$$

Let $J_R=J_{QV}-J_{QB}J_{P\theta}^{-1}J_{PV}$, a voltage stability index (VSI) for the whole system can be defined as:

$$VSI=\min\frac{det(J_R)}{[adj(J_R)]_{ii}}\quad i=1,2,\ldots,N \tag{30}$$

where N is the number of buses; $det(J_R)$ is the determinant of J_R; and $adj(J_R)=det(J_R)J_R^{-1}$. VSI can be used to indicate how close the system is to voltage instability. The bigger VSI is, the more stable the system is. When VSI approaches zero, the system will lose voltage stability [49].

VI. Proposed Blackout Model

Figure 4 illustrates the proposed cascading failure model.

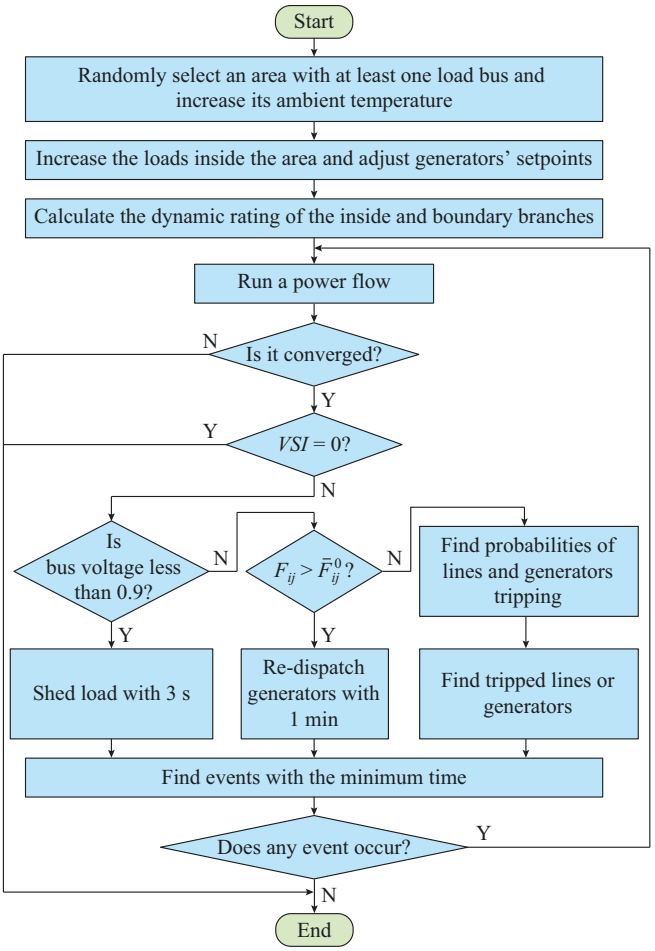

Fig. 4. Flowchart of cascading failure model.

By utilizing our proposed model, we can realistically model cascading failures and capture what has happened in previous blackouts. Even though the system is $N-1$ secure, cascading failure can still be initiated and then propagated in a large area of the system. The reasons are as follows.

1) Although load forecasting is used for day-ahead generation purchase and reactive power management, due to the uncertainties such as unexpected temperature disturbances, the actual load may be different from the forecasted load, hence system operation conditions are changed.

2) Under different weather conditions, the actual line rating could change significantly due to a number of processes such as the overheating of a transmission line or the sagging of the line to vegetation. An $N-1$ secure system with initial line ratings may not still be $N-1$ secure with the reduced dynamic line ratings due to temperature increase.

3) The initiating events have important geographical corre-

lations due to external weather conditions such as temperature disturbance. Increased line flow will occur owing to temperature increase with load increase and line rating decrease at the same time, greatly increasing the line tripping probability inside or on the boundary of an area with temperature disturbances. Generators inside the area with temperature disturbance also have the increasing possibility of being disconnected due to load increase as well as the reduction of reactive supply from the outside system after tie line disconnection. The proposed cascading failure model considers the correlations between different events such as line outage, generator tripping, and undervoltage of load buses, which may lead to extensive outage propagation even if the system is initially $N-1$ secure without any temperature disturbance.

VII. Results

The proposed model is implemented in MATLAB for the RTS-96 3-area system [50] based on MATPOWER [51]. There are 73 buses and 120 branches in the system, and the total load is 8550 MW. Compared with the initial model, each reactor of 100 Mvar at buses 106, 206, and 306 is split into two 50 Mvar at each extremity of the cable. These reactors are considered to be automatically disconnected in case of the outage of the corresponding cable. The pre-contingency steady state is based on a preventive-security-constrained optimal power flow so that the system is $N-1$ secure [52]. All tests are carried out on a 3.20 GHz Intel(R) Core(TM) i7-8700 based desktop.

A. Parameter Setting

We set $k^{pf}=0.001$ for all buses [8]; $K=1.5$ in Section II-D for lines [53]; $\underline{K}_{Q_i}=1.5\underline{Q}_i$ if $\underline{Q}_i<0$ and $\underline{K}_{Q_i}=-0.5$ if $\underline{Q}_i=0$ as in Section II-E; and $\overline{K}_{Q_i}=1.5\overline{Q}_i$. Besides, $\epsilon=0.01$ for lines [53]; and $\underline{\epsilon}=-0.01\underline{Q}_i$ and $\overline{\epsilon}=0.01\overline{Q}_i$ for generators. We choose $p_1=0.001$, $p_2=0.3$, and $p_3=1$ [53]. For generators, we choose $p_4=0.001$ to consider hidden failures, $p_5=0.3$, and $p_6=1$. For re-dispatch, we set $\eta=1.05$ [54]. To calculate the dynamic line ratings, we consider $\alpha_{ij}=1$.

B. Typical Simulation Without Operator Re-dispatch

Buses 207 and 208 are selected as the internal buses and their initial temperatures are set to be $T_{0,high}=24.21$ ℃. For a temperature disturbance, we increase the temperature of the selected area to $T=T_{0,high}+10$ ℃. As in Table I, after the temperature increases, the active and reactive power at these two buses also increase. The line flows and the dynamic line ratings of the boundary and internal branches are listed in Table II. After the temperature increases, the line flows increase while $\overline{F}_{ij}^{d}$ decreases compared with $\overline{F}_{0,ij}$, and branches 207-208 and 208-209 become overloaded.

If dynamic line rating is not considered, $F_{ij}(T_{ij})$ for all lines are less than $\overline{F}_{0,ij}$, and the line tripping probability is as low as p_1. And the generator tripping probability is equal to p_4. However, it is totally different if the dynamic line rating is considered.

TABLE I
Internal Buses with Their Active and Reactive Power Without Operator Re-dispatch

Inside bus	$P(T_i^0)$ (MW)	$P(T_i)$ (MW)	$Q(T_{0,i})$ (Mvar)	$Q(T_i)$ (Mvar)
207	125	189.79	25	48.08
208	171	259.63	35	66.76

TABLE II
Initial Flows, Flow After Temperature Increases, and Dynamic Line Rating of Boundary and Internal Branches Without Operator Re-dispatch

Branch	$F_{ij}(T_{0,ij})$	$\overline{F}_{0,ij}$	$F_{ij}(T_{ij})$	$\overline{F}_{ij}^{d}(T_{ij})$
(207, 208)	53.24	175	148.89	147.40
(208, 209)	96.41	190	175.07	173.21
(208, 210)	82.77	190	161.81	173.45

When operator re-dispatch is not modeled, the event sequence simulated from the proposed model is shown in Fig. 5, in which the number next to the tripped line or generator indicates the sequence of the event. After the temperature of the selected area increases, branch 207-208 will be tripped by the probability of 0.3. In the simulation, it is tripped after 991.40 s, which leads to the undervoltage of bus 208 and the islanding of the generators at bus 207. Then the cascading failure gradually propagates to the other parts of the system, leading to 35 line outages and 19 generator trippings at 12 generator buses. The line outages, generator outages, and undervoltage buses during the blackout are shown in Fig. 6.

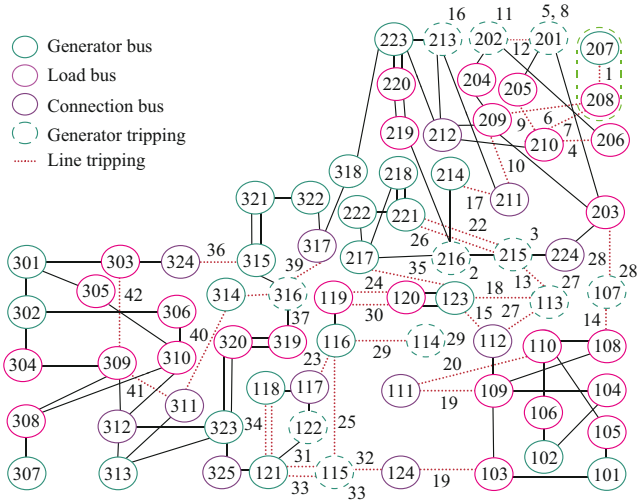

Fig. 5. A typical blackout in RTS-96 system simulated by proposed model without operator re-dispatch.

For generator outages, the involved generator buses are shown. Since one generator bus has several generators connected to it, it may appear more than once (such as generator bus 201).

The total load during the blackout is shown in Fig. 7(a). Three seconds after the first line tripping, part of the load at bus 208 is shed due to undervoltage. Due to islanding and undervoltage, load shedding becomes much faster after 8036

s. VSI during the cascading event is shown in Fig. 7(b). Under normal operation conditions, VSI is 14.68, and when the blackout propagates, it gradually decreases. At 11454.2 s, VSI decreases from 2.02 to 1.39. Figure 7(c) shows the voltage of four vulnerable buses (buses 303, 305, 306, and 324) over time. After VSI reduces to 1.39, the voltages at the vulnerable buses begin to drop significantly before voltage collapse finally occurs at 12657 s.

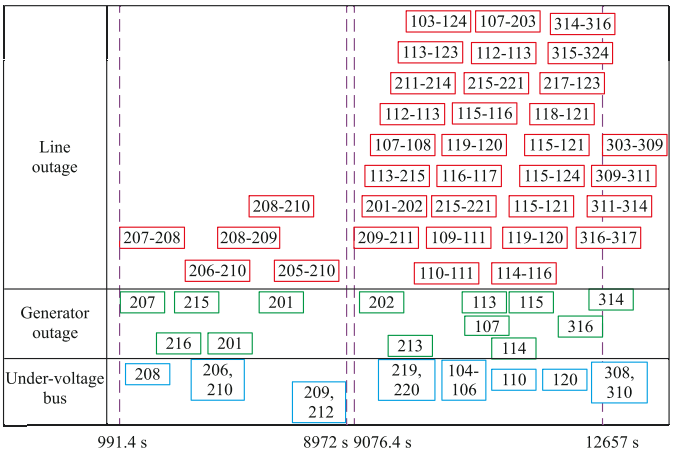

Fig. 6. Events in typical case without operator re-dispatch.

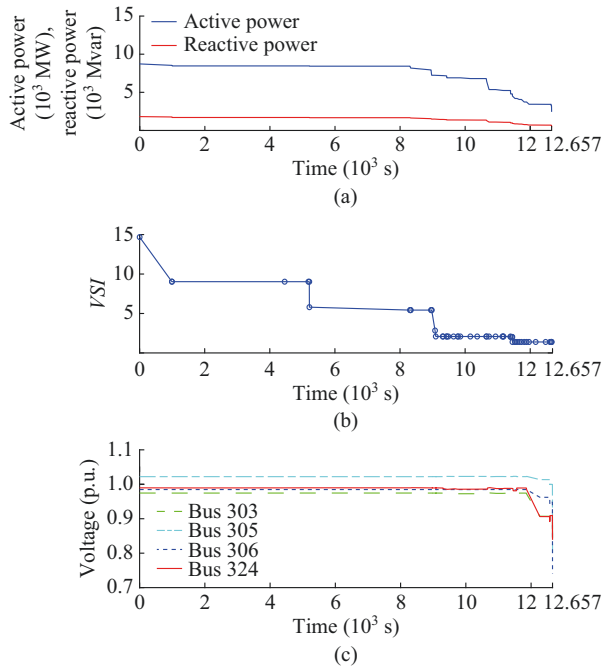

Fig. 7. Total load, VSI, and voltage at vulnerable buses in typical case without operator re-dispatch. (a) Total load. (b) VSI. (c) Voltage at vulnerable buses.

C. Typical Simulation with Operator Re-dispatch

In this case, buses 304, 305, 306, 309, 310, and 314 are chosen as the internal buses and their initial temperatures are $T^0_{high} = 24.21$ °C. The temperature of the selected area increases to $T = T^0_{high} + 10$ °C to simulate a temperature disturbance. As shown in Table III, the active and reactive power at the internal buses increase due to temperature increase. The line flows and dynamic line ratings of the boundary and internal branches are shown in Table IV. The line flow of branch 314-316 becomes higher than its dynamic line rating and is to be tripped by the probability of 0.32. In the simulation, it is tripped after 798.34 s and initiates a cascading failure. Figure 8 shows the process of a typical blackout in RTS-96 system when simulated by proposed model with operator re-dispatch, in which the number next to the tripped line or generator indicates the sequence of the event. The tripping of branch 314-316 leads to the overloading of branch 312-323 which is tripped after 54.2 s. These events result in the undervolatge of buses 303, 309, and 324 at 855.54 s and the overloading of branches 313-323 at 915.54 s. The operator re-dispatch at 975.54 s eliminates the overloading of branches 313-323, but the generator at bus 314 within the selected area is tripped at 2415.75 s due to overexcitation and cascading failure spreads to the other parts of the system, causing 19 line outages and 14 generator trippings at 11 generator buses. The operator re-dispatch, line outages, generator outages, and undervoltage buses during the blackout are illustrated in Fig. 9.

TABLE III
INTERNAL BUSES WITH THEIR ACTIVE AND REACTIVE POWER WITH OPERATOR RE-DISPATCH

Inside bus	$P(T_{0,i})$ (MW)	$P(T_i)$ (MW)	$Q(T_{0,i})$ (Mvar)	$Q(T_i)$ (Mvar)
304	74	112.4	15	29.9
305	71	107.8	14	27.4
306	141	214.1	28	54.7
309	175	265.7	36	69.5
310	195	296.1	40	77.3
314	194	294.6	39	75.9

TABLE IV
INITIAL FLOWS, FLOW AFTER TEMPERATURE RISES, AND DYNAMIC LINE RATING OF BOUNDARY AND INTERNAL BRANCHES IN TYPICAL CASE WITH OPERATOR RE-DISPATCH

Branch	$F_{ij}(T^0_{ij})$	$\overline{F}^0_{ij}$	$F_{ij}(T_{ij})$	$\overline{F}^d_{ij}(T_{ij})$
(305, 301)	48.3	175	88.1	167.7
(304, 302)	39.4	175	67.3	172.5
(306, 302)	41.1	175	66.5	160.2
(309, 303)	20.8	175	40.9	158.4
(304, 309)	49.2	175	82.7	147.4
(305, 310)	25.3	175	47.4	147.4
(306, 310)	150.4	180	151.6	152.4
(309, 308)	97.4	190	81.8	174.3
(309, 311)	146.5	400	191.1	352.5
(309, 312)	165.1	400	211.2	353.7
(310, 311)	193.4	400	266.3	351.3
(310, 312)	216.5	400	288.2	342.5
(314, 316)	354.7	500	498.5	492.4

The total load during the blackout is shown in Fig. 10(a). After two line trippings, the undervoltage happens at buses 303, 309, and 324, and part of the load at these buses is

shed due to the undervoltage. VSI during the cascading event is shown in Fig. 10(b). At 5378.5 s, VSI drops from 2.72 to 0.97. Figure 10(c) presents the voltage of eight vulnerable buses (buses 303, 308, 309, 310, 311, 312, 313, and 324), some of which are inside the selected area. It is noticed that after VSI decreases to 0.97, the voltage at the vulnerable buses begin to drop remarkably before the voltage eventually collapses at 5381.5 s.

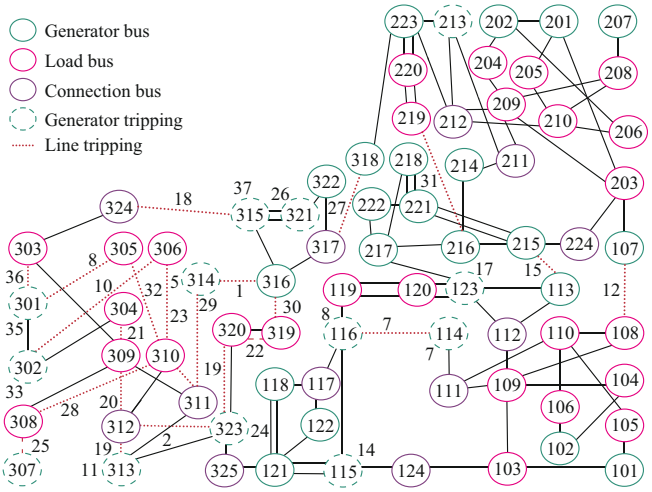

Fig. 8. A typical blackout in RTS-96 system simulated by proposed model with operator re-dispatch.

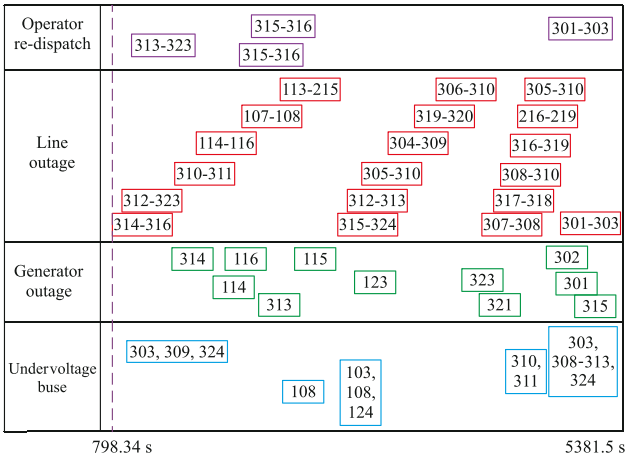

Fig. 9. Illustration of operator re-dispatch, line outages, generator outages, and undervoltage buses during blackout.

D. Number of Simulations

Since many random factors could affect the simulation of cascading failures, we set $\gamma=0.07$, $\Delta T=11$ ℃ and run the model for different times in order to decide a number for which the variance of the simulation results is small enough. Figure 11 shows the average values and the standard deviations of the number of outages for different number of simulations. After 10000 simulations, the average value of outages (both line and generator outages) stabilizes and the standard deviation of the number of outages decreases to a very small value. For the other parameters of γ and ΔT, the results are very similar and are thus not given. Therefore, in this paper, we run the model for 10000 times.

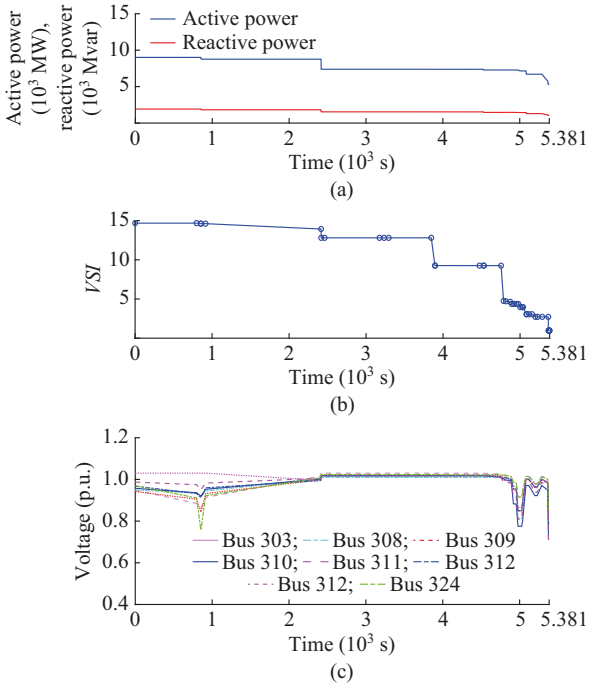

Fig. 10. Total load, VSI, and voltage at vulnerable buses with operator re-dispatch. (a) Total load. (b) VSI. (c) Voltage at vulnerable buses.

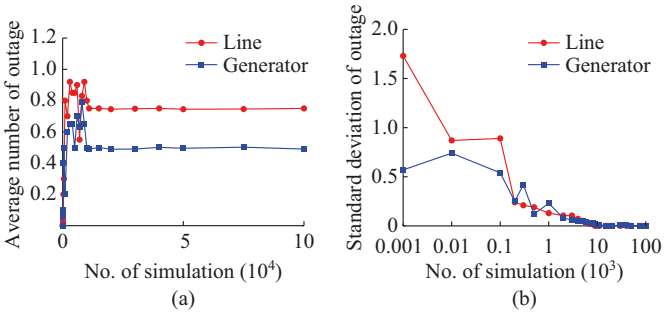

Fig. 11. Average values and standard deviations of number of outages for different number of simulations. (a) Average value. (b) Standard deviation.

E. Impact of Temperature Disturbances and Size of Selected Area

We set $\gamma=0.07$ and run the proposed model for 10000 times with randomly selected areas, in which the ambient temperature increases from $T_{0,high}$ or decreases from $T_{0,low}$ by ΔT. Figure 12 shows the average number of outages with different temperature disturbances. When the temperature increases, the total number of line and generator outages is small when $\Delta T\leq 11$ ℃, and will grow quickly when $\Delta T>$ 11 ℃. Therefore, $\Delta T=11$ ℃ can be inferred as the critical temperature disturbance. As presented in Fig. 13, if the temperature decreases, while the load increases, the dynamic line rating also increases. Therefore, the total number of line and generator outages is always low.

We also analyze the impact of the size of the selected area when the temperature increases with $\Delta T=11$ ℃, and a random area is selected with a different value of γ. The results in Fig. 14 indicate that by enlarging the selected area, the number of line and generator outages increases. The number of line and generator outages significantly increases when $\gamma>$

0.07. Therefore, $\gamma = 0.07$ can be inferred as the critical size.

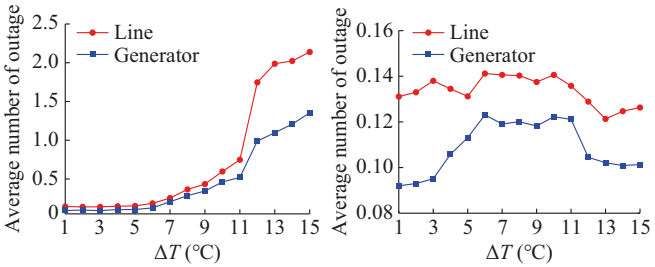

Fig. 12. Average number of outages with different temperature disturbances. (a) Increasing temperature. (b) Decreasing temperature.

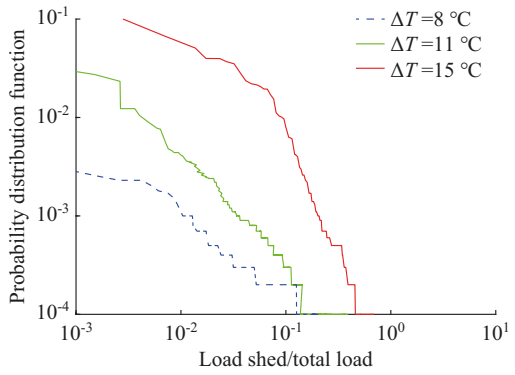

Fig. 13. Distribution of load shed with different temperature increase disturbances.

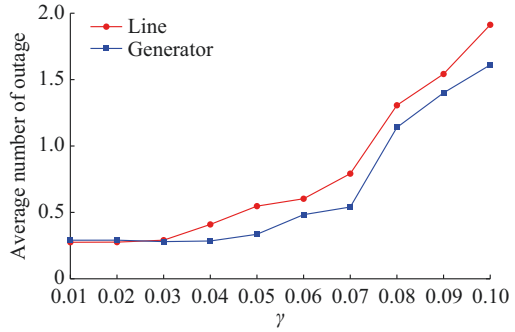

Fig. 14. Average number of outages in different areas.

Figure 15 shows the pairs of critical temperature versus critical area size. It can be seen that as the critical size of the selected area increases, the critical temperature disturbance decreases.

F. Identifying the Most Vulnerable Buses and Locations

The vulnerability of the buses and locations is dependent on the temperature disturbance and the size of the selected area. Therefore, to effectively identify the most vulnerable locations, we run the model 10000 times for all combinations of $\Delta T = \{8\ °C, 10\ °C, 11\ °C, 15\ °C\}$ and $\gamma = \{0.05, 0.06, 0.07, 0.08\}$ around every load bus. Also,we can identify the vulnerable buses in very diverse failure scenarios. Figure 16(a) shows the average number of outages for load buses and Fig. 16(b) shows the ratio between load shed and total load for load buses. We can see that the load buses 208, 308, 305, 210, 209, 306, 309, and 310 are more vulnerable than the other buses, and the temperature disturbances around these buses lead to much more line and generator outages and load shed.

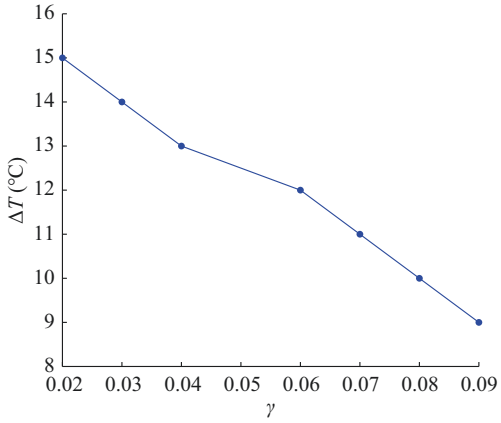

Fig. 15. Critical temperature versus critical area size.

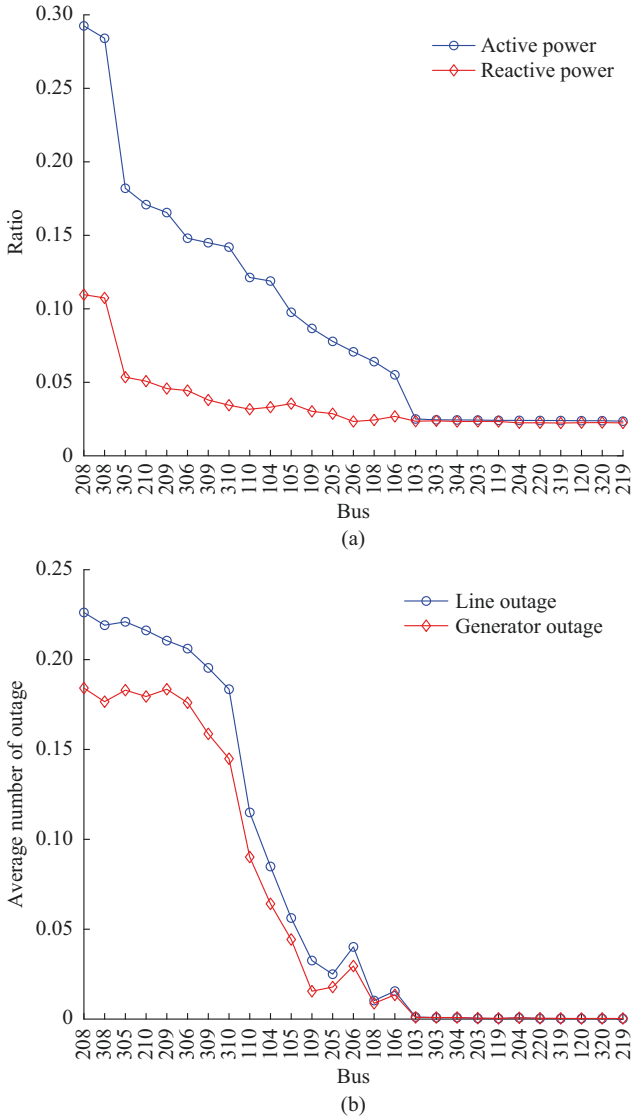

Fig. 16. Identification of vulnerable buses. (a) Average number of outages for load buses. (b) Ratio between load shed and total load for load buses.

G. Impact of Control Strategies

In Section VII-B, if the operator re-dispatch is modeled by considering the initial line rating, at 8972 s, the operator re-dispatch is performed since the power flow of some branches exceeds their initial capacities and the potential outage of branch 209-211 would take 104.4 s which is longer than 60 s, i.e., the time required for operator re-dispatch. After the operator re-dispatch, the cascading failure stops.

Besides, we set $\Delta T = 11$ ℃, $\gamma = 0.07$, and run simulations for 10000 times with or without the operator re-dispatch. Figure 17 shows the distribution of number of line and generator outages with or without the operator re-dispatch. It is clear that by implementing the re-dispatch strategy using F_{ij}^0, the number of line and generator outages decreases. Besides, by considering dynamic line rating for re-dispatch, the risk can be reduced much more significantly.

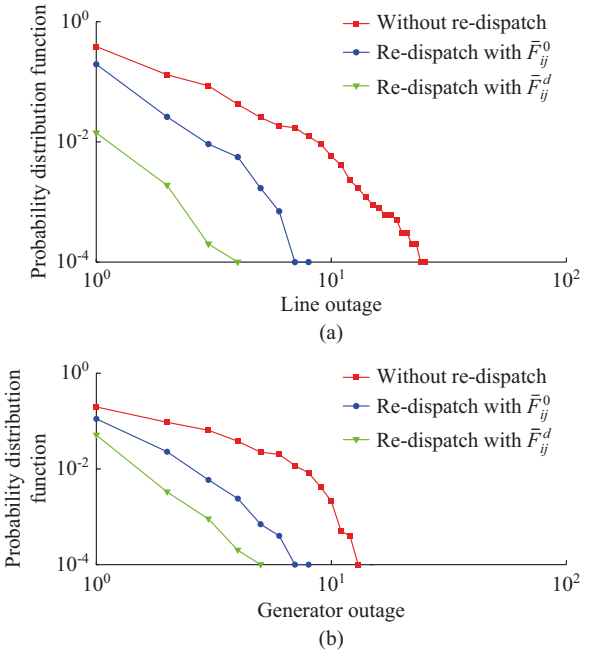

Fig. 17. Distribution of number of line and generator outages with or without re-dispatch. (a) Line outage. (b) Generator outage.

VIII. Conclusion

In this paper, a blackout model is proposed, considering the changes of load and dynamic line rating due to ambient temperature disturbance. We apply the proposed model to the RTS-96 3-area system and find that temperature disturbance can lead to correlated load change and line tripping, which will together contribute to voltage collapse. Based on the proposed model, we identify critical temperature change, critical area with temperature disturbance, and most vulnerable buses, and compare the effectiveness of different control strategies.

In this paper, the major mechanisms that could lead to the initiation and propagation of cascading failures are the load increase and line rating decrease caused by ambient temperature disturbances, the coupling between different events such as line outages, generator outages, undervoltage of load buses, and the consequent voltage collapse. As the penetration of renewable generation is quickly increasing, the future power system will be even more impacted by external factors such as weather conditions. This is because compared with traditional fossil fuel based generation, the renewable generation, which is mostly power-electronic-interfaced, depends more on weather conditions, and is more sensitive to the system disturbances such as voltage disturbances caused by transmission outages due to lightning or wildfire [55]-[57]. The blackout model proposed in this paper can be further extended for future power system with high penetration of renewable generation to evaluate the cascading failure risk, identify critical components that play important roles in outage initiation and propagation, and develop effective mitigation strategies to significantly reduce the cascading failures.

References

[1] K. Sun, Y. Hou, W. Sun *et al*., *Power System Control Under Cascading Failures: Understanding, Mitigation, and System Restoration*, Hoboken: Wiley-IEEE Press, 2019.
[2] P. Praks, V. Kopustinskas, and M. Masera, "Monte-Carlo-based reliability and vulnerability assessment of a natural gas transmission system due to random network component failures," *Sustainable and Resilient Infrastructure*, vol. 2, no. 3, pp. 97-107, Jul. 2017.
[3] M. Theoharidou, M. Kandias, and D. Gritzalis, "Securing transportation-critical infrastructures: trends and perspectives," in *Global Security, Safety and Sustainability & e-Democracy*, Berlin: Springer, 2011, pp. 171-178.
[4] S. Hong, H. Yang, T. Zhao *et al*., "Epidemic spreading model of complex dynamical network with the heterogeneity of nodes," *International Journal of Systems Science*, vol. 47, no. 11, pp. 2745-2752, Aug. 2016.
[5] S. Hong, C. Lv, Zhao *et al*., "Cascading failure analysis and restoration strategy in an interdependent network," *Journal of Physics A: Mathematical and Theoretical*, vol. 49, no. 19, p. 195101, Apr. 2016.
[6] M. A. Gilani, A. Kazemi, and M. Ghasemi, "Distribution system resilience enhancement by microgrid formation considering distributed energy resources," *Energy*, vol. 191, p. 116442, Jan. 2020.
[7] S. Hong, J. Zhu, L. A. Braunstein *et al*., "Cascading failure and recovery of spatially interdependent networks," *Journal of Physics A: Mathematical and Theoretical*, vol. 2017, no. 10, p. 103208, Oct. 2017.
[8] B. Liscouski and W. Elliot, "Final report on the August 14, 2003 blackout in the United States and Canada: causes and recommendations," *A Report to US Department of Energy*, vol. 40, no. 4, p. 86, Apr. 2004.
[9] Federal Energy and Regulatory Commission and North American Electric Reliability Corporation, "Arizona-Southern California outages on September 8, 2011: causes and recommendations," Washington DC: FERC and NERC, 2012.
[10] L. Lai, H. Zhang, C. Lai *et al*., "Investigation on July 2012 Indian blackout," in *Proceedings of 2013 International Conference on Machine Learning and Cybernetics*, Tianjin, China, Jul. 2013, pp. 92-97.
[11] H. Haggi, M. Song, W. Sun *et al*., "A review of smart grid restoration to enhance cyber-physical system resilience," in *Proceedings of IEEE Innovative Smart Grid Technologies-Asia (ISGT Asia)*, Chengdu, China, May 2019, pp. 4008-4013.
[12] D. S. Kirschen, D. Jayaweera, D. P. Nedic *et al*., "A probabilistic indicator of system stress," *IEEE Transactions on Power Systems*, vol. 19, no. 3, pp. 1650-1657, Aug. 2004.
[13] A. Phadke and J. S. Thorp, "Expose hidden failures to prevent cascading outages in power systems," *IEEE Computer Applications in Power*, vol. 9, no. 3, pp. 20-23, Jul. 1996.
[14] J. Chen, J. S. Thorp, and I. Dobson, "Cascading dynamics and mitigation assessment in power system disturbances via a hidden failure model," *International Journal of Electrical Power & Energy Systems*, vol. 27, no. 4, pp. 318-326, May 2005.
[15] I. Dobson, B. A. Carreras, and D. E. Newman, "A loading-dependent model of probabilistic cascading failure," *Probability in the Engineering and Informational Sciences*, vol. 19, no. 1, pp. 15-32, Jan. 2005.
[16] B. A. Carreras, D. E. Newman, I. Dobson *et al*., "Validating OPA with WECC data," in *Proceedings of 46th Hawaii International Conference*

System and Sciences, Hawaii, USA, Jan. 2013, pp. 2197-2204.
[17] S. Mei, Y. Ni, G. Wang *et al*., "A study of self-organized criticality of power system under cascading failures based on AC-OPF with voltage stability margin," *IEEE Transactions on Power Systems*, vol. 23, no. 4, pp. 1719-1726, Nov. 2008.
[18] J. Song, E. Cotilla-Sanchez, G. Ghanavati *et al*., "Dynamic modeling of cascading failure in power systems," *IEEE Transactions on Power Systems*, vol. 31, no. 3, pp. 2085-2095, May 2015.
[19] I. Dobson, A. Flueck, S. Aquiles-Perez *et al*., "Towards incorporating protection and uncertainty into cascading failure simulation and analysis," in *Proceedings of IEEE International Conference on Probabilistic Methods Applied to Power Systems (PMAPS)*, Idaho, USA, Jan. 2018, pp. 1-5.
[20] J. Qi and S. Pfenninger, "Controlling the self-organizing dynamics in a sandpile model on complex networks by failure tolerance," *EPL (Europhysics Letters)*, vol. 111, no. 3, p. 38006, Aug. 2015.
[21] J. Qi, I. Dobson, and S. Mei, "Towards estimating the statistics of simulated cascades of outages with branching processes," *IEEE Transactions on Power Systems*, vol. 28, no. 3, pp. 3410-3419, Aug. 2013.
[22] I. Dobson, "Estimating the propagation and extent of cascading line outages from utility data with a branching process," *IEEE Transactions on Power Systems*, vol. 27, no. 4, pp. 2146-2155, Nov. 2012.
[23] J. Qi, W. Ju, and K. Sun, "Estimating the propagation of interdependent cascading outages with multi-type branching processes," *IEEE Transactions on Power Systems*, vol. 32, no. 2, pp. 1212-1223, Mar. 2017.
[24] J. Qi, K. Sun, and S. Mei, "An interaction model for simulation and mitigation of cascading failures," *IEEE Transactions on Power Systems*, vol. 30, no. 2, pp. 804-819, Mar. 2015.
[25] W. Ju, J. Qi, and K. Sun, "Simulation and analysis of cascading failures on an NPCC power system test bed," in *Proceedings of 2015 IEEE PES General Meeting*, Denver, USA, Aug. 2015, pp. 1-5.
[26] J. Qi, J. Wang, and K. Sun, "Efficient estimation of component interactions for cascading failure analysis by EM algorithm," *IEEE Transactions on Power Systems*, vol. 33, no. 3, pp. 3153-3161, May 2018.
[27] W. Ju, K. Sun, and J. Qi, "Multi-layer interaction graph for analysis and mitigation of cascading outages," *IEEE Journal on Emerging and Selected Topics in Circuits and Systems*, vol. 7, no. 2, pp. 239-249, Jun. 2017.
[28] J. Qi, "Utility outage data driven interaction networks for cascading failure analysis and mitigation," *IEEE Transactions on Power Systems*, doi: 10.1109/TPWRS.2020.3015380.
[29] K. Zhou, I. Dobson, Z. Wang *et al*., "A Markovian influence graph formed from utility line outage data to mitigate large cascades," *IEEE Transactions on Power Systems*, vol. 35, no. 4, pp. 3224-3235, Jul. 2020.
[30] D. N. Kosterev, C. W. Taylor, and W. A. Mittelstadt, "Model validation for the August 10, 1996 WSCC system outage," *IEEE Transactions on Power Systems*, vol. 14, no. 3, pp. 967-979, Aug. 1999.
[31] C. W. Taylor and D. C. Erickson, "Recording and analyzing the July 2 cascading outage (Western USA power system)," *IEEE Computer Applications in Power*, vol. 10, no. 1, pp. 26-30, Jan. 1997.
[32] M. Anghel, K. A. Werley, and A. E. Motter, "Stochastic model for power grid dynamics," in *Proceedings of 2007 40th Annual Hawaii International Conference on System Sciences (HICSS' 07)*, Big Island, USA, Jan. 2007, pp. 113-113.
[33] J. Qi, S. Mei, and F. Liu, "Blackout model considering slow process," *IEEE Transactions on Power Systems*, vol. 28, no. 3, pp. 3274-3282, Aug. 2013.
[34] P. Henneaux, P. E. Labeau, and J. C. Maun, "Blackout probabilistic risk assessment and thermal effects: impacts of changes in generation," *IEEE Transactions on Power Systems*, vol. 28, no. 4, pp. 4722-4731, Nov. 2013.
[35] R. Yao and K. Sun, "Towards simulation and risk assessment of weather-related outages," *IEEE Transactions on Smart Grid*, vol. 10, no. 4, pp. 4391-4400, Jul. 2019.
[36] I. Dobson, N. K. Carrington, K. Zhou *et al*., "Exploring cascading outages and weather via processing historic data," arXiv preprint arXiv: 1709.09079, 2017.
[37] D. Rick, "Deriving the haversine formula," in The Math Forum, April, Apr. 1999.
[38] P. J. Robinson, "Modeling utility load and temperature relationships for use with long-lead forecasts," *Journal of Applied Meteorology*, vol. 36, no. 5, pp. 591-598, May 1997.
[39] S. Mirasgedis, Y. Sarafidis, E. Georgopoulou *et al*., "Models for mid-term electricity demand forecasting incorporating weather influences," *Energy*, vol. 31, no. 2, pp. 208-227, Feb. 2006.
[40] S. Mirasgedis, Y. Sarafidis, E. Georgoupolou *et al*., "Modeling framework for estimating impacts of climate change on electricity demand at regional level: case of Greece," *Energy Conversion and Management*, vol. 48, no. 5, pp. 1737-1750, May 2007.
[41] J. D. Glover, M. S. Sarma, and T. Overbye, *Power System Analysis and Design*, New York: Cengage Learning, 2012.
[42] A. Michiorri, H. M. Nguyen, S. Alessandrini *et al*., "Forecasting for dynamic line rating," *Renewable and Sustainable Energy Reviews*, vol. 52, pp. 1713-1730, Dec. 2015.
[43] P. Kundur, N. J. Balu, and M. G. Lauby, *Power System Stability and Control*, New York: McGraw-hill, 1994.
[44] B. Otomega and T. van Cutsem, "Undervoltage load shedding using distributed controllers," *IEEE Transactions on Power Systems*, vol. 22, no. 4, pp. 1898-1907, Oct. 2007.
[45] T. Van Cutsem, M. Glavic, W. Rosehart *et al*., "Test systems for voltage stability analysis and security assessment," *IEEE Transactions on Power Systems*, vol. 35, no. 5, pp. 4078-4087, Sept. 2020.
[46] Y. Xue, M. Thakhar, J. C. Theron *et al*., "Review of the breaker failure protection practices in utilities," in *Proceedings of 65th Annual Conference for Protective Relay Engineers*, Texas, USA, Apr. 2012, pp. 260-268.
[47] M. J. Eppstein and P. D. Hines, "A "random chemistry" algorithm for identifying collections of multiple contingencies that initiate cascading failure," *IEEE Transactions on Power Systems*, vol. 27, no. 3, pp. 1698-1705, Aug. 2012.
[48] V. Doifode, M. V. Aranke, S. M. Choudhary *et al*. (2016, Mar.). An overview of classes & grouping in generator protection at VIPL (Nagpur). [Online]. Available: https://www. researchgate. net/publication/ 320200511_An_Overview_of_Classes_Grouping_in_Generator_Protec - tion_at_V_I_P_L_Nagpur
[49] H. Li, A. Bose, and V. M. Venkatasubramanian, "Wide-area voltage monitoring and optimization," *IEEE Transactions on Smart Grid*, vol. 7, no. 2, pp. 785-793, Mar. 2015.
[50] R. Force, "The IEEE reliability test system-1996," *IEEE Transactions on Power Systems*, vol. 14, no. 3, pp. 1010-1020, Aug. 1999.
[51] R. D. Zimmerman, C. E. Murillo-Sánchez, and R. J. Thomas, "Matpower: steady-state operations, planning, and analysis tools for power systems research and education," *IEEE Transactions on Power Systems*, vol. 26, no. 1, pp. 12-19, Jun. 2010.
[52] P. Henneaux, E. Ciapessoni, D. Cirio *et al*., "Benchmarking quasi-steady state cascading outage analysis methodologies," in *Proceedings of IEEE International Conference on Probabilistic Methods Applied to Power Systems (PMAPS)*, Idaho, USA, Jun. 2018, pp. 1-6.
[53] S. T. Lee, "Estimating the probability of cascading outages in a power grid," in *Proceedings of 16th Power Systems Computation Conference*, Glasgow, UK, Jul. 2008, pp. 14-18.
[54] R. Yao, S. Huang, K. Sun *et al*., "A multi-timescale quasi-dynamic model for simulation of cascading outages," *IEEE Transactions on Power Systems*, vol. 31, no. 4, pp. 3189-3201, Jul. 2015.
[55] North American Electric Reliability Council, "1200 MW fault induced solar photovoltaic resource interruption disturbance report," Tech. Rep., Jul. 2017.
[56] R. Yan, T. K. Saha, F. Bai *et al*., "The anatomy of the 2016 South Australia blackout: a catastrophic event in a high renewable network," *IEEE Transactions on Power Systems*, vol. 33, no. 5, pp. 5374-5388, Sept. 2018.
[57] N. G. ESO, "Technical report on the events of 9 August 2019," Tech. Rep., Sept. 2019.

Seyyed Rashid Khazeiynasab received the B.Sc. degree from Shiraz University, Shiraz, Iran, and the M.Sc. degree from Sharif University of Technology, Tehran, Iran, in 2011 and 2013, respectively. He joined the University of Central Florida, Orlando, USA, in August 2018. Currently, he is pursuing his Ph.D. degree in electrical engineering. His research interests include power system modeling, cascading blackouts and parameter estimation.

Junjian Qi received the B.E. degree in electrical engineering from Shandong University, Jinan, China, in 2008, and the Ph.D. degree in electrical engineering from Tsinghua University, Beijing, China, in 2013. He is currently an Assistant Professor with the Department of Electrical and Computer Engineering, Stevens Institute of Technology, Hoboken, USA. He was the recipient of the NSF CAREER award in 2020 and is an Associate Editor for the IEEE Access. His research interests include cascading blackouts, microgrid control, cyber-physical systems, and synchrophasors.